

Article

# [<sup>18</sup>F]fallypride-PET/CT Analysis of the Dopamine D<sub>2</sub>/D<sub>3</sub> Receptor in the Hemiparkinsonian Rat Brain Following Intrastratial Botulinum Neurotoxin A Injection

Teresa Mann <sup>1,\*</sup>, Jens Kurth <sup>2</sup> , Alexander Hawlitschka <sup>1</sup>, Jan Stenzel <sup>3</sup>, Tobias Lindner <sup>3</sup> , Stefan Polei <sup>3</sup>, Alexander Hohn <sup>2</sup>, Bernd J. Krause <sup>2</sup> and Andreas Wree <sup>1</sup>

<sup>1</sup> Institute of Anatomy, Rostock University Medical Center, Gertrudenstrasse 9, 18057 Rostock, Germany; alexander.hawlitschka@med.uni-rostock.de (A.H.); andreas.wree@med.uni-rostock.de (A.W.)

<sup>2</sup> Department of Nuclear Medicine, Rostock University Medical Centre, Gertrudenplatz 1, 18057 Rostock, Germany; jens.kurth@med.uni-rostock.de (J.K.); alexander.hohn@med.uni-rostock.de (A.H.); bernd.krause@med.uni-rostock.de (B.J.K.)

<sup>3</sup> Core Facility Multimodal Small Animal Imaging, Rostock University Medical Center, Schillingallee 69a, 18057 Rostock, Germany; Jan.Stenzel@med.uni-rostock.de (J.S.); tobias.lindner@med.uni-rostock.de (T.L.); stefan.polei@gmx.de (S.P.)

\* Correspondence: teresa.mann@med.uni-rostock.de; Tel.: +49-381-494-8433

Received: 30 January 2018; Accepted: 4 March 2018; Published: 6 March 2018

**Abstract:** Intrastratial injection of botulinum neurotoxin A (BoNT-A) results in improved motor behavior of hemiparkinsonian (hemi-PD) rats, an animal model for Parkinson's disease. The caudate-putamen (CPU), as the main input nucleus of the basal ganglia loop, is fundamentally involved in motor function and directly interacts with the dopaminergic system. To determine receptor-mediated explanations for the BoNT-A effect, we analyzed the dopamine D<sub>2</sub>/D<sub>3</sub> receptor (D<sub>2</sub>/D<sub>3</sub>R) in the CPU of 6-hydroxydopamine (6-OHDA)-induced hemi-PD rats by [<sup>18</sup>F]fallypride-PET/CT scans one, three, and six months post-BoNT-A or -sham-BoNT-A injection. Male Wistar rats were assigned to three different groups: controls, sham-injected hemi-PD rats, and BoNT-A-injected hemi-PD rats. Disease-specific motor impairment was verified by apomorphine and amphetamine rotation testing. Animal-specific magnetic resonance imaging was performed for co-registration and anatomical reference. PET quantification was achieved using PMOD software with the simplified reference tissue model 2. Hemi-PD rats exhibited a constant increase of 23% in D<sub>2</sub>/D<sub>3</sub>R availability in the CPU, which was almost normalized by intrastratial application of BoNT-A. Importantly, the BoNT-A effect on striatal D<sub>2</sub>/D<sub>3</sub>R significantly correlated with behavioral results in the apomorphine rotation test. Our results suggest a therapeutic effect of BoNT-A on the impaired motor behavior of hemi-PD rats by reducing interhemispheric changes of striatal D<sub>2</sub>/D<sub>3</sub>R.

**Keywords:** D<sub>2</sub>/D<sub>3</sub> receptors; hemiparkinsonian rat model; Botulinum neurotoxin A; basal ganglia; striatum; Parkinson's disease; small animal imaging; PET/CT; [<sup>18</sup>F]fallypride; MRI

## 1. Introduction

Positron emission tomography (PET) using the radioligand [<sup>18</sup>F]fallypride enables in vivo detection of disease-specific alterations of the dopaminergic system, more precisely of D<sub>2</sub>/D<sub>3</sub> receptor (D<sub>2</sub>/D<sub>3</sub>R) availability. Small animal PET hybrid tomographs allow imaging and quantification of D<sub>2</sub>/D<sub>3</sub>R binding by the use of [<sup>18</sup>F]fallypride in rodent models of neurodegenerative disorders like Parkinson's disease (PD) [1–3]. [<sup>18</sup>F]fallypride is characterized by high sensitivity and selectivity for D<sub>2</sub>R; for instance, administration of the D<sub>2</sub>R antagonist haloperidol blocked specific [<sup>18</sup>F]fallypride

binding in the mouse caudate–putamen (CPu) by 95% [4,5]. Besides specific binding to D<sub>2</sub>R, [<sup>18</sup>F]fallypride displays affinity to the D<sub>2</sub>-like D<sub>3</sub>R, about 20% of the radioligand bind to D<sub>3</sub>R in vivo in small animals [6]. In PD a drastic loss of striatal dopamine (DA) caused by progressing degeneration of dopaminergic neurons in the substantia nigra pars compacta (SNpc) results in imbalanced neurotransmitter systems and underlies motor complications. Moreover, due to DA depletion and the subsequent missing inhibition of striatal cholinergic interneurons, hypercholinism is an additional feature of PD exacerbating motor impairment [7,8]. Interestingly, there are physiological bidirectional regulating effects of the cholinergic and dopaminergic system [9] via complex involvement of muscarinic and nicotinic receptors on DA release from dopaminergic terminals [10,11].

For causal analysis and development of novel therapeutics for PD in preclinical research the experimental hemiparkinsonian (hemi-PD) is an accepted animal model [12]. Unilateral injection of 6-hydroxydopamine (6-OHDA) into the medial forebrain bundle (MFB) of rats provokes rapid dopaminergic depletion by auto-oxidation and consequent oxidative stress [13]. The near-complete loss of dopaminergic neurons in the SNpc via retrograde axonal transport of the toxin 6-OHDA after stereotaxic injection into the MFB mimics a late stage of PD [14]. Current therapeutic strategies for PD focus primarily on compensation of DA in the striatum (caudate–putamen, CPu) by either DA precursors [15,16] or DA receptor agonists [17]. Though, clinical efficiency is limited and chronic administrations leads to severe side effects like motor fluctuations and dyskinesia [18,19]. Other therapeutic options target the cholinergic system mostly by blocking muscarinic receptors or by inhibition of cholinesterase [20,21]. Systemic administration of anticholinergic substances causes severe side effects like confusion, dry mouth, blurred vision, and cognitive impairment [22].

Recently, we demonstrated that local injection of the anticholinergic Botulinum neurotoxin A (BoNT-A) significantly improved D<sub>2</sub>R agonist-induced asymmetric rotational behavior in hemi-PD rats [23–26]. BoNT-A acts mainly on cholinergic neurons and inhibits distribution of acetylcholine into the synaptic cleft via cleavage of the synaptosomal-associated protein of 25-kDa (SNAP25) [27–29]. The intracerebral injection of BoNT-A avoids severe side effects in both the central and peripheral nervous system [23]. Notably, intrastriatal application of BoNT-A does not cause cytotoxicity [30] or impaired cognition [24] in rats. As known from other medical implementation, BoNT-A demonstrates a transient therapeutic effect in hemi-PD rats that lasts up to six months post-injection [23,31]. To examine the longitudinal cellular mechanisms of the positive BoNT-A effect on receptor level, we performed [<sup>18</sup>F]fallypride-PET/CT scans one, three, and six months post-BoNT-A or -sham-BoNT-A injection and quantified D<sub>2</sub>/D<sub>3</sub>R availability in controls, sham-injected hemi-PD rats, and BoNT-A-injected hemi-PD rats.

## 2. Results

D<sub>2</sub>/D<sub>3</sub>R availability was analyzed longitudinally in controls (sham-6-OHDA + sham-BoNT-A, *n* = 9), sham-injected hemi-PD rats (6-OHDA + sham-BoNT-A, *n* = 7) and BoNT-A-injected hemi-PD rats (6-OHDA + BoNT-A, *n* = 10) by dynamic [<sup>18</sup>F]fallypride-PET/CT scans.

### 2.1. Immunohistochemistry and Behavioral Testing

To qualitatively verify successful 6-OHDA-induced dopaminergic deafferentation we performed tyrosine hydroxylase (TH) immunostaining (for dopaminergic neurons). TH-reaction in the left and right CPu and SN of control rats (sham-6-OHDA + sham-BoNT-A) showed no loss of TH-reaction (Figure 1a,b). In hemi-PD rats (6-OHDA + sham-BoNT-A) an ipsilateral loss of almost all TH-immunoreactivity was visible in the CPu and SN, indicating dopaminergic deafferentation in the CPu due to dopaminergic cell loss in the SN (Figure 1c,d), and BoNT-A injection in hemi-PD rats (6-OHDA + BoNT-A) did not demonstrate an additive effect on these reaction patterns (Figure 1e,f).

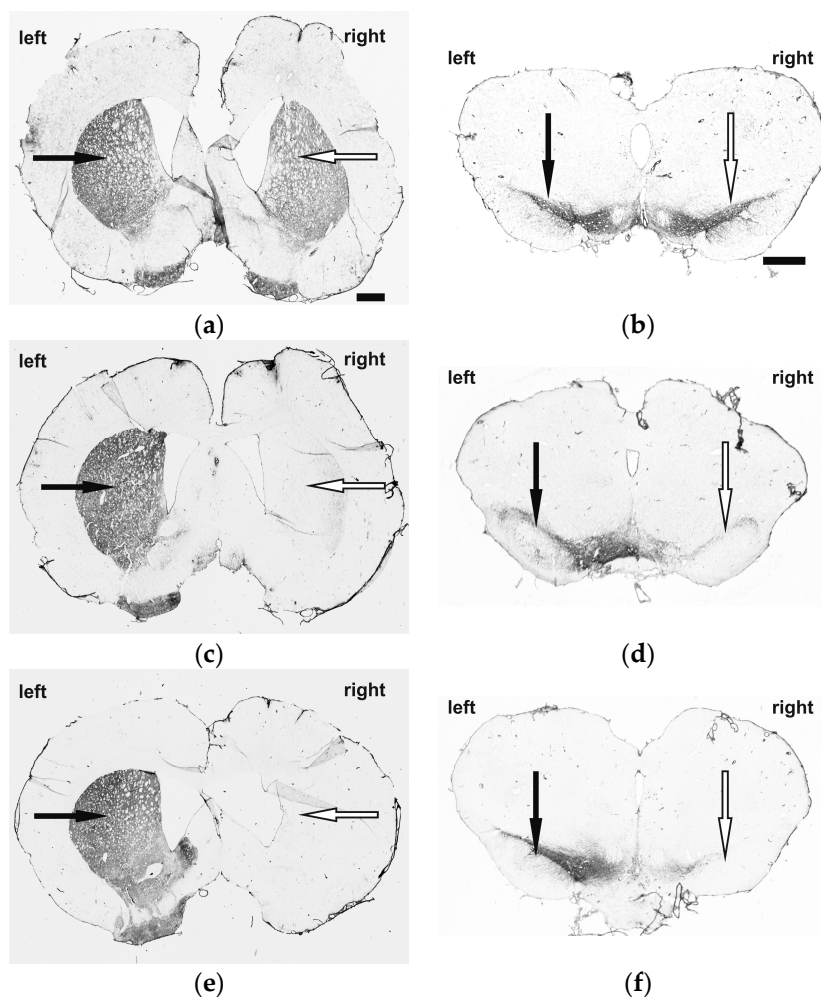


**Figure 1.** TH-immunoreactivity in the telencephalon (left column) and the mesencephalon (right column) of (a,b) controls (sham-6-OHDA + sham-BoNT-A) (c,d) sham-injected hemi-PD rats (6-OHDA + sham-BoNT-A) and (e,f) BoNT-A-injected hemi-PD rats (6-OHDA + BoNT-A). 6-OHDA or sham-6-OHDA was unilaterally injected into the MFB of the right hemisphere and BoNT-A was injected ipsilateral at two sites into the CPu. Controls showed symmetric TH pattern in the CPu (a,c,e; black (left) and white (right) arrow) and SN (b,d,f; black (left) and white (right) arrow), sham-injected hemi-PD rats demonstrated an almost complete loss of TH-positive cells in the CPu and SN and BoNT-A injection did not influence these findings in hemi-PD rats. The scale bar applies for a–f = 1 mm.

Asymmetric rotations of hemi-PD rats were tested using apomorphine- and amphetamine-induced rotations one month after 6-OHDA lesion. Also, the positive effect of intrastrially injected BoNT-A on drug-induced rotations was analyzed two weeks after administration. All hemi-PD rats exhibited distinct apomorphine-induced rotations contralateral to the 6-OHDA lesion before BoNT-A or sham-BoNT-A injection of  $8.2 \pm 3.6$  rpm (6-OHDA + sham-BoNT-A) and  $9.2 \pm 3.0$  rpm (6-OHDA + BoNT-A), controls did not show rotational behavior (sham-6-OHDA + sham-BoNT-A) (Figure 2a). Sham injection in hemi-PD rats slightly decreased rotations to  $4.6 \pm 2.5$  rpm (6-OHDA + sham-BoNT-A) and did not affect the behavior of controls (sham-6-OHDA + sham-BoNT-A). Following BoNT-A injection rotational behavior was reversed in hemi-PD rats to  $2.2 \pm 2.1$  rpm (6-OHDA + BoNT-A). The positive motor effect of BoNT-A in hemi-PD rats was significant compared to sham injections ( $p = 0.021$ ) (Figure 2a). Before BoNT-A or sham-BoNT-A injection amphetamine administration caused ipsilateral rotations in hemi-PD rats of  $-7.3 \pm 3.4$  rpm (6-OHDA + sham-BoNT-A) and  $-6.6 \pm 2.9$  rpm (6-OHDA + BoNT-A) but not

in controls (sham-6-OHDA + sham-BoNT-A) (Figure 2b). After BoNT-A or sham-BoNT-A injection asymmetric rotational behavior was with  $-12.0 \pm 6.3$  rpm (6-OHDA + BoNT-A) and  $-10.3 \pm 3.5$  rpm (6-OHDA + sham-BoNT-A) further increased and BoNT-A effect was compared to sham injection not significantly abolished. Sham-BoNT-A injection in controls (sham-6-OHDA + sham-BoNT-A) did not result in ipsilateral rotations (Figure 2b).

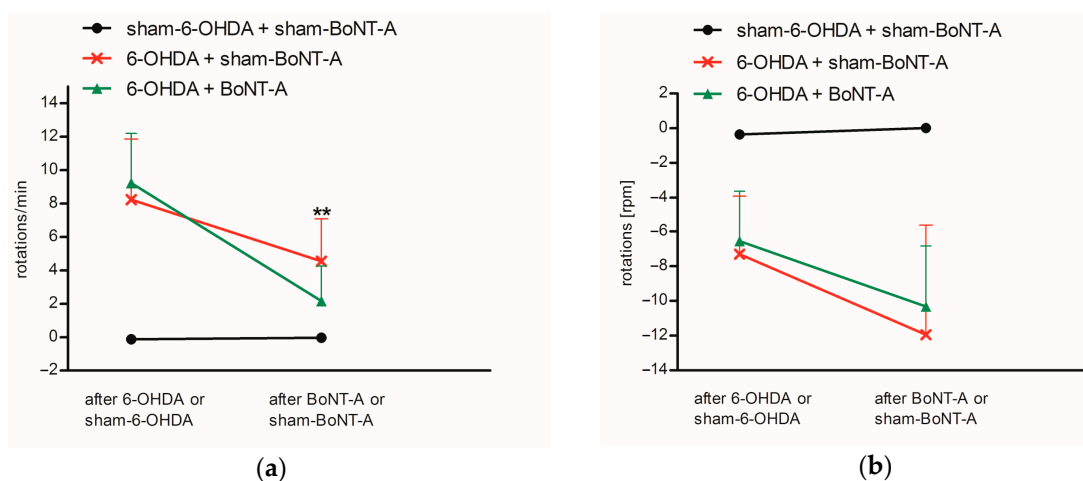


**Figure 2.** Results of the rotational behavior in (a) apomorphine- and (b) amphetamine-induced testing for controls (sham-6-OHDA + sham-BoNT-A), sham-injected hemi-PD rats (6-OHDA + sham-BoNT-A) and BoNT-A-injected hemi-PD rats (6-OHDA + BoNT-A) displayed after 6-OHDA or sham-6-OHDA and BoNT-A or sham-BoNT-A injection. Rotations contralateral to the injection side (clockwise) are displayed with negative algebraic signs, anti-clockwise rotations with positive algebraic signs. Controls did not demonstrate designated rotational behavior, hemi-PD rats exhibited strong asymmetric drug-induced rotations that were almost completely abolished after BoNT-A injection in apomorphine testing and slightly abolished in amphetamine testing. Significance is displayed as \*\*  $p < 0.01$ .

## 2.2. Striatal $D_2/D_3R$ Availability

Qualitative analysis with parametric mapping of non-displaceable binding potential ( $BP_{nd}$ ) revealed no obvious interhemispheric differences for controls (sham-6-OHDA + sham-BoNT-A). However, increased signals in the right CPU of hemi-PD rats were visible (6-OHDA + sham-BoNT-A) compared to the unaffected side. This visual right–left difference was diminished after BoNT-A injection into the right CPU of hemi-PD rats (6-OHDA + BoNT-A) (Figure 3a–c).



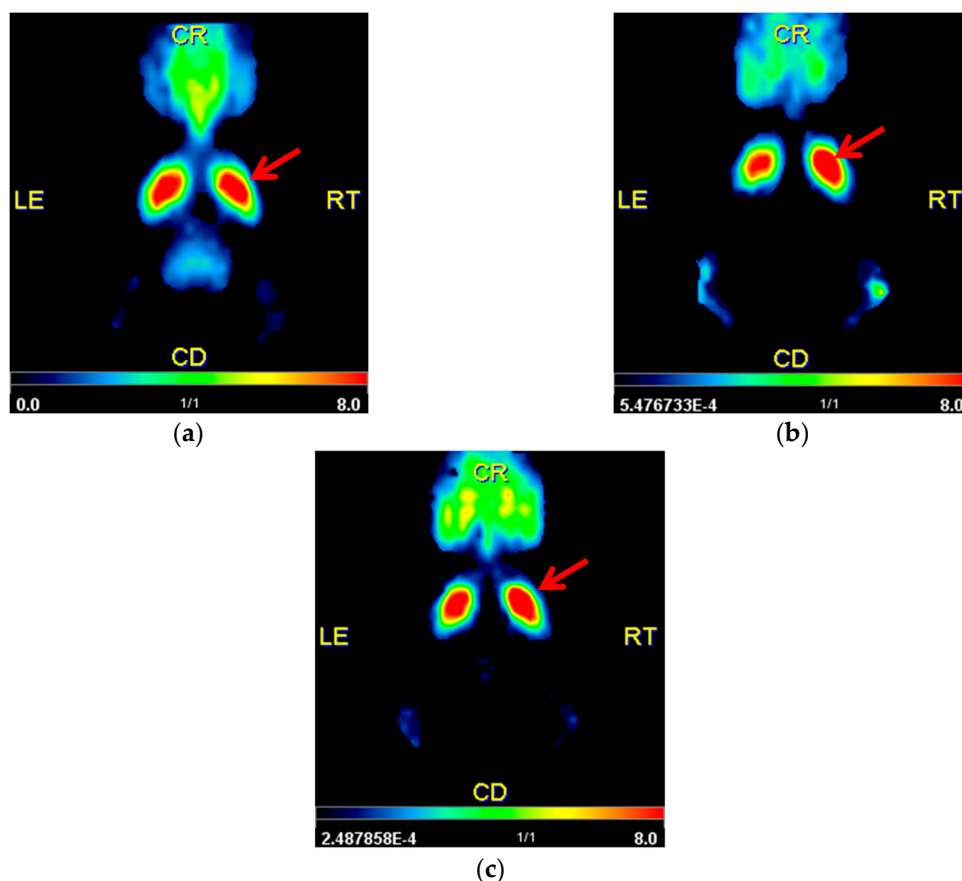


**Figure 3.** Qualitative analysis using pixel-wised parametric mapping for the parameter  $BP_{nd}$  showing the left and right CPu in transversal sections for (a) controls (sham-6-OHDA + sham-BoNT-A) (b) sham-injected hemi-PD rats (6-OHDA + sham-BoNT-A) and (c) BoNT-A-injected hemi-PD rats (6-OHDA + BoNT-A) one month after BoNT-A or sham-BoNT-A injection. A representative animal of each experimental group was used. Controls did not reveal visual side differences, an increased signal of  $BP_{nd}$  distribution in the right CPu of hemi-PD rats was clearly visible and BoNT-A injection normalized the increased signal in hemi-PD rats. The right CPu is marked with a red arrow.

For quantification the simplified reference tissue model 2 (SRTM2) was applied and  $BP_{nd}$  was estimated separately for the left and right striatum. Controls (sham-6-OHDA + sham-BoNT-A) revealed no relative interhemispheric right–left differences: mean  $BP_{nd}$  of  $4.2 \pm 0.8/4.2 \pm 0.8$  (left/right CPu) one month post-sham-BoNT-A injection,  $3.8 \pm 0.8/3.7 \pm 0.9$  (left/right CPu) three months post-sham-BoNT-A injection and  $4.1 \pm 0.7/4.1 \pm 0.7$  (left/right CPu) six months post-sham-BoNT-A injection were found (Figure 4a,c; Table 1). Hemi-PD rats that received sham-BoNT-A injection (6-OHDA + sham-BoNT-A) exhibited strong interhemispheric right–left differences of about 23%: kinetic analysis resulted in mean  $BP_{nd}$  values of  $4.4 \pm 0.6/5.5 \pm 0.9$  (left/right CPu) one month post-sham-BoNT-A injection,  $4.4 \pm 1.1/5.5 \pm 1.3$  (left/right CPu) three months post-sham-BoNT-A injection, and  $4.8 \pm 1.0/5.7 \pm 1.0$  (left/right CPu) six months post-sham-BoNT-A injection. The contralateral CPu was never affected and displayed very stable  $BP_{nd}$  throughout all experimental groups and scanning time points (Figure 4a–c; Table 1). The increase in  $BP_{nd}$  in the right CPu of hemi-PD rats (6-OHDA + sham-BoNT-A) was significant compared to the left CPu of the same experimental group one month post-sham-BoNT-A injection ( $p = 0.047$ ) (Figure 4a) and compared to the right CPu of controls (sham-6-OHDA + sham-BoNT-A) at all 3 examined time points ( $p = 0.03$ ,  $p = 0.064$ ,  $p = 0.039$ ) (Figure 4a–c). BoNT-A injection in hemi-PD rats (6-OHDA + BoNT-A) reduced relative interhemispheric right–left difference to about 13.4%: quantification revealed mean  $BP_{nd}$  of

$4.7 \pm 0.4/5.3 \pm 0.5$  (left/right CPu) one month post-BoNT-A injection,  $4.4 \pm 1.0/5.0 \pm 1.2$  (left/right CPu) three months post-BoNT-A injection and  $4.4 \pm 1.0/5.1 \pm 1.1$  (left/right CPu) six months post-BoNT-A injection (Figure 4a–c; Table 1). The BoNT-A effect was significant compared to the ipsilateral CPu of controls (sham-6-OHDA + sham-BoNT-A) one month post-BoNT-A injection ( $p = 0.0087$ ) and showed a transient course throughout the timeline (Figure 4a–c). A list of all individual values for BP<sub>nd</sub> expressing D<sub>2</sub>/D<sub>3</sub>R availability separately for the left and right CPu and the relative interhemispheric right–left difference in each of the 26 analyzed rats is displayed in Table 1.

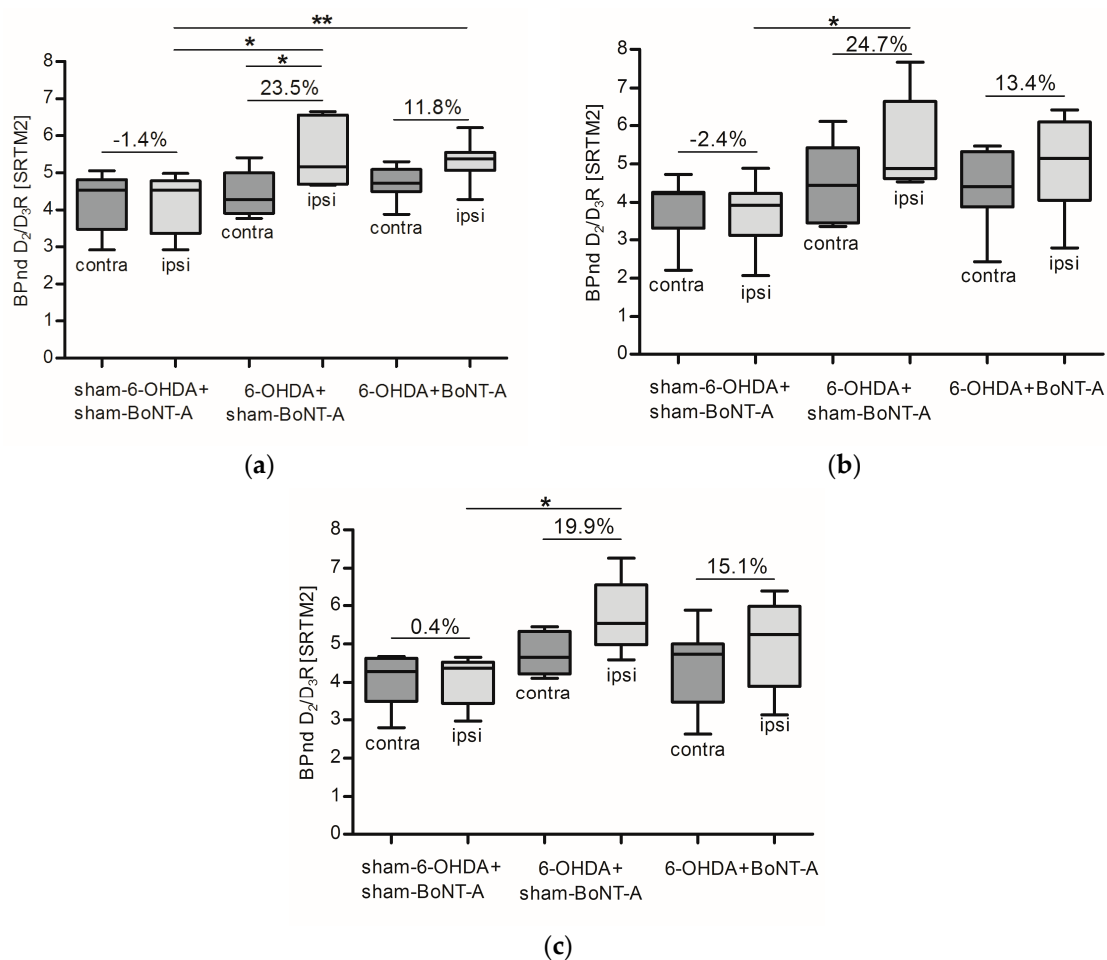


**Figure 4.** Box plots for BP<sub>nd</sub> values of D<sub>2</sub>/D<sub>3</sub>R depicting median and interquartile ranges separately for the contralateral (dark grey) and ipsilateral (light grey) CPu for controls (sham-6-OHDA + sham-BoNT-A), sham-injected hemi-PD rats (6-OHDA + sham-BoNT-A) and BoNT-A-injected hemi-PD rats (6-OHDA + BoNT-A) (a) one month, (b) three months, and (c) six months post-BoNT-A or -sham-BoNT-A injection. D<sub>2</sub>/D<sub>3</sub>R availability was consistently symmetric in controls, increased in sham-injected hemi-PD rats at all analyzed time points and was reduced to nearly normal values after BoNT-A injection in hemi-PD rats. Significance is displayed as \*  $p < 0.05$ , \*\*  $p < 0.01$ .

**Table 1.** Summary of all single BP<sub>nd</sub> values of D<sub>2</sub>/D<sub>3</sub>R for the left and right CPu and the interhemispheric difference relative to the left hemisphere in (%) analyzed in controls (sham-6-OHDA + sham-BoNT-A), sham-injected hemi-PD rats (6-OHDA + sham-BoNT-A) and BoNT-A-injected hemi-PD rats (6-OHDA + BoNT-A). Data are shown for all three PET/CT scans (PET/CT 1: one month post-BoNT-A or sham-BoNT-A, PET/CT 2: three months post-BoNT-A or -sham-BoNT-A, PET/CT 3: six months post-BoNT-A or -sham-BoNT-A). \* indicate that no data were analyzed due to incorrect tracer injection or no data acquisition.

Group	PET/CT 1			PET/CT 2			PET/CT 3		
	BP <sub>nd</sub> Left	BP <sub>nd</sub> Right	(%)	BP <sub>nd</sub> Left	BP <sub>nd</sub> Right	(%)	BP <sub>nd</sub> Left	BP <sub>nd</sub> Right	(%)
sham-6-OHDA + sham-BoNT-A	5.06	4.98	−1.66	2.21	2.07	−6.35	*	*	*
sham-6-OHDA + sham-BoNT-A	2.92	2.92	−0.01	3.74	3.93	5.21	4.56	4.44	−2.66
sham-6-OHDA + sham-BoNT-A	4.53	4.53	−0.04	2.87	2.78	−3.37	3.29	3.23	−1.84
sham-6-OHDA + sham-BoNT-A	4.58	4.59	0.28	4.25	4.15	−2.28	4.65	4.53	−2.46
sham-6-OHDA + sham-BoNT-A	4.03	3.80	−5.71	4.24	3.93	−7.22	4.07	4.02	−1.36
sham-6-OHDA + sham-BoNT-A	*	*	*	3.81	3.46	−9.32	4.68	4.52	−3.47
sham-6-OHDA + sham-BoNT-A	*	*	*	4.73	4.89	3.34	2.80	2.97	6.23
sham-6-OHDA + sham-BoNT-A	*	*	*	4.27	4.32	1.04	4.50	4.66	3.60
sham-6-OHDA + sham-BoNT-A	*	*	*	4.23	4.13	−2.48	4.07	4.30	5.66
Mean  ± SD	4.2 ± 0.8	4.2 ± 0.8	1.4 ± 2.5	3.8 ± 0.8	3.7 ± 0.9	2.4 ± 4.9	4.1 ± 0.7	4.1 ± 0.7	0.4 ± 4.0
6-OHDA + sham-BoNT-A	4.86	6.53	34.37	6.11	7.67	25.53	4.11	4.59	11.53
6-OHDA + sham-BoNT-A	5.41	6.65	22.90	*	*	*	4.66	5.54	19.07
6-OHDA + sham-BoNT-A	3.77	4.67	23.84	3.35	4.54	35.56	5.45	7.26	33.13
6-OHDA + sham-BoNT-A	4.08	4.71	15.53	4.44	4.88	10.04	5.21	5.83	11.98
6-OHDA + sham-BoNT-A	3.96	4.79	21.02	*	*	*	*	*	*
6-OHDA + sham-BoNT-A	4.49	5.54	23.50	4.74	5.64	18.80	4.33	5.37	23.95
6-OHDA + sham-BoNT-A	*	*	*	3.53	4.71	33.46	*	*	*
Mean  ± SD	4.4 ± 0.6	5.5 ± 0.9	23.5 ± 6.1	4.4 ± 1.1	5.5 ± 1.3	24.7 ± 14.8	4.8 ± 1.0	5.7 ± 1.0	19.9 ± 11.4
6-OHDA + BoNT-A	4.58	5.33	16.19	*	*	*	3.30	3.92	18.62
6-OHDA + BoNT-A	4.54	4.90	7.94	5.47	6.10	11.59	*	*	*
6-OHDA + BoNT-A	5.07	5.54	9.23	4.41	5.15	16.68	2.63	3.13	19.11
6-OHDA + BoNT-A	5.09	5.42	6.39	2.43	2.79	14.93	4.74	5.25	10.77
6-OHDA + BoNT-A	4.85	5.43	11.80	*	*	*	5.88	6.38	8.56
6-OHDA + BoNT-A	4.37	5.15	17.86	*	*	*	4.86	6.03	24.05
6-OHDA + BoNT-A	4.59	5.12	11.55	3.88	4.06	4.77	3.63	3.87	6.45
6-OHDA + BoNT-A	3.88	4.28	10.26	4.33	5.13	18.59	5.00	5.93	18.53
6-OHDA + BoNT-A	5.30	6.22	17.22	4.94	5.26	6.49	4.58	5.23	14.22
6-OHDA + BoNT-A	5.10	5.59	9.74	5.32	6.41	20.38	5.01	5.78	15.38
Mean  ± SD	4.7 ± 0.4	5.3 ± 0.5	11.8 ± 4.0	4.4 ± 1.0	5.0 ± 1.2	13.4 ± 6.0	4.4 ± 1.0	5.1 ± 1.1	15.1 ± 5.7

### 2.3. Correlation of $D_2/D_3R$ Side Differences and Behavior

A possible correlation of the degree of interhemispheric differences in  $D_2/D_3R$  availability and apomorphine-induced rotations for controls (sham-6-OHDA + sham-BoNT-A), sham-injected hemi-PD rats (6-OHDA + sham-BoNT-A) and BoNT-A-injected hemi-PD rats (6-OHDA + BoNT-A) was examined one month post-BoNT-A or -sham-BoNT-A injection. Controls (sham-6-OHDA + sham-BoNT-A) did not demonstrate right–left differences or rotational behavior. With increasing right–left differences contralateral rotations of hemi-PD rats (6-OHDA + sham-BoNT-A) increased and also the normalizing effect on interhemispheric  $D_2/D_3R$  differences after BoNT-A injection (6-OHDA + BoNT-A) was connected with behavior. A highly significant relationship between increasing right–left differences, expressing a higher  $D_2/D_3R$  availability in the right CPU, and the apomorphine-induced rotational behavior was found ( $p = 0.0007$ ) (Figure 5).

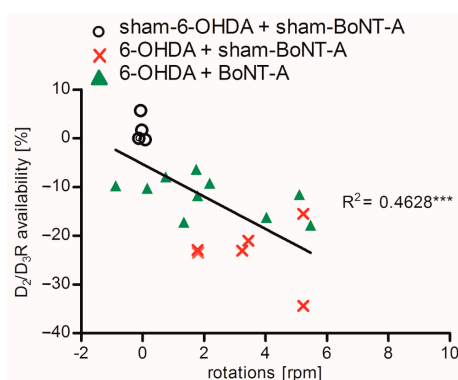


**Figure 5.** Linear correlation of right–left differences of  $D_2/D_3R$  availability in (%) and apomorphine-induced rotations one month after BoNT-A or sham-BoNT-A injection for controls (sham-6-OHDA + sham-BoNT-A), sham-injected hemi-PD rats (6-OHDA + sham-BoNT-A) and BoNT-A-injected hemi-PD rats (6-OHDA + BoNT-A). Controls did neither demonstrate interhemispheric differences nor rotational behavior. With increasing right–left differences also asymmetric rotations increased in hemi-PD rats and both was normalized after BoNT-A injection. Significance is displayed as \*\*\*  $p < 0.001$ .

### 3. Discussion

In this study we examined cellular mechanisms of the positive motor effect of intrastrially injected BoNT-A by [ $^{18}F$ ]fallypride PET/CT scans in hemi-PD rats, as BoNT-A was previously demonstrated to abolish apomorphine-induced rotational behavior in 6-OHDA-lesioned [23–26]. The control group respected the entire surgical procedure as the minimal lesion caused by the insertion of the syringe could lead to changes in receptor binding sites [32,33]. We did not include an experimental group studying BoNT-A in sham-lesioned rats in our design as we assumed that BoNT-A would not alter per se the expression of  $D_2/D_3$  receptors. Indeed, we have previously performed extensive in vitro analysis of  $D_2/D_3$  receptors as well as apomorphine-induced rotational behavior in BoNT-A-injected rats earlier and did not find major effects [31].

Hemi-PD rats demonstrated a constant contralateral rotational behavior after apomorphine injection and rather inconsistent amphetamine-induced rotations four weeks after 6-OHDA lesion (Figure 2a,b). A period of four weeks before behavioral testing was left to ensure maximum dopaminergic deafferentation, as dopaminergic cell death [34] as well as consequent plasticity effects [31] last up to four weeks after injection of 6-OHDA. Notably, increasing right–left differences of  $D_2/D_3R$  availability significantly correlated with increasing asymmetry in apomorphine-induced rotations (Figure 5). Rotational tests using the  $D_2$  agonist apomorphine or the DA releaser amphetamine are commonly used to detect the degree of dopaminergic deafferentation in hemi-PD rats. As apomorphine acts on increased striatal  $D_2/D_3R$  in the DA-depleted CPU of hemi-PD rats [35–37],

it leads to a larger inhibition of the right CPu and as a consequence to an elevated motor urge to the contralateral side. Resulting rotations to the left of more than four rotations per minute confirm dopaminergic degeneration of more than 90% [25,38–40]. Amphetamine induces DA release from nerve terminals and strongly affects the non-lesioned hemisphere of hemi-PD rats, which begin to turn to the ipsilateral side of the 6-OHDA lesion [41]. In line with our findings, another study demonstrated that apomorphine but not amphetamine is a reliable indicator for maximal dopaminergic cell death in hemi-PD rats [42].

Dynamic [ $^{18}\text{F}$ ]fallypride PET/CT scans over 90 min revealed an increase of 23% in  $\text{D}_2/\text{D}_3\text{R}$  availability being consistent up to six months post-6-OHDA lesion and a normalization of this pathological imbalance after BoNT-A injection into the CPu of hemi-PD rats (Figures 3 and 4; Table 1). Unlike [ $^{11}\text{C}$ ]raclopride, [ $^{18}\text{F}$ ]fallypride is not easily displaced by endogenous DA, as demonstrated in monkey [43], human [44] and rat brain [45]. To cover the transient effect of BoNT-A demonstrated previously [23], we performed longitudinal measurements using [ $^{18}\text{F}$ ]fallypride in the same rodent. This seemed feasible as repeated measurements with [ $^{18}\text{F}$ ]fallypride PET/CT exhibited only small variations in mice [5] and also in our study, controls (sham-6-OHDA + sham-BoNT-A) did not show variations in  $\text{BP}_{\text{nd}}$  comparing the three PET/CT scanning time points (Figures 3a and 4a–c; Table 1).

Our finding of a constant increase of about 23% in  $\text{D}_2/\text{D}_3\text{R}$  availability in hemi-PD rats is in line with a number of similar studies both in vitro and in vivo. Unilateral injection of 6-OHDA into the MFB or SNpc of rats resulted in a consistent increase of  $\text{D}_2\text{R}$  density of 20% to 40% subject to the injected dosage and survival time analyzed using in vitro autoradiography [35,46–50]. Also, in vivo PET/CT analyses with [ $^{11}\text{C}$ ]raclopride and [ $^{18}\text{F}$ ]fallypride are in accordance with our results. [ $^{11}\text{C}$ ]raclopride PET demonstrated an ipsilateral increase of 17% to 27.7% [2] and approximately 35% [51] in  $\text{D}_2\text{R}$  availability in hemi-PD rats after MFB injection and an increase of 23% [52] and 16.6% [53] after 6-OHDA lesion of the SNpc. [ $^{18}\text{F}$ ]fallypride PET/CT scans revealed an 12% increase in  $\text{D}_2/\text{D}_3\text{R}$  availability in hemi-PD rats after injection of 6-OHDA into the CPu [2].

Intrastrially injections with BoNT-A significantly reduced the pathologically increased  $\text{D}_2/\text{D}_3\text{R}$  availability in hemi-PD rats (Figures 3c and 4) and significantly abolished apomorphine-induced rotations (Figure 2a). Apomorphine-induced rotations were also moderately decreased after sham-BoNT-A injection in hemi-PD rats. This effect is likely to be caused by minimal mechanical damage caused by insertion of the cannula into the CPu and injection of sham solution. One might argue that the positive BoNT-A effect is caused by simple striatal cell death after BoNT-A injection, as  $\text{D}_2/\text{D}_3\text{R}$  are localized on medium spiny neurons (MSN), presynapses of cholinergic interneurons and boutons of dopaminergic afferents in the CPu [54–56]. Previously we demonstrated that BoNT-A injection did neither cause striatal neuronal loss or reduced volume [26] nor death of cholinergic interneurons in the CPu [30]. The positive BoNT-A effect diminished with increasing post-injection time. The BoNT-A effect on  $\text{D}_2/\text{D}_3\text{R}$  in hemi-PD rats has been analyzed before in a quantitative in vitro autoradiography study demonstrating a normalizing effect, which significantly correlates with apomorphine-induced rotations [31].

A preceding study performed [ $^{11}\text{C}$ ]raclopride PET to analyze the effect of BoNT-A on pathological increased  $\text{D}_2/\text{D}_3\text{R}$  and found a positive effect on pathological increased  $\text{D}_2\text{R}$  availability in hemi-PD rats [3]. Here, we extended this experimental setup by introducing a control group (sham-6-OHDA + sham-BoNT-A) to investigate both ipsi- and contralateral effects of tissue damage by cannula injection and increased group size to substantiate possible significant effects. Moreover, we used the more specific radioligand [ $^{18}\text{F}$ ]fallypride instead of [ $^{11}\text{C}$ ]raclopride and conducted animal-specific MRI scans for co-registration with CT-corrected PET data to improve data analysis by making use of the high morphologic resolution of MRI.

Quantification was subsequently performed using SRTM2 [57] for kinetic modeling, having the advantage of no need for arterial blood sampling and being established especially for neuroimaging studies [58]. Application of kinetic models allows quantitative determination of transfer rates and provides in depth understanding of physiological parameters. The cerebellum was used as the



reference region being devoid of D<sub>2</sub>/D<sub>3</sub>R [59] and being validated as a suitable reference region for D<sub>2</sub>/D<sub>3</sub>R before [60–62]. As spatial resolution of PET scans is a limiting factor especially in small animals [63], we used animal-specific MRI scans for spatial normalization, thus high precision of Voxels of interest (VOI) delineation and almost full recovery could be guaranteed in our study. Partial volume effects (PVE) occur mostly in structures being smaller than about 2 times of the width at half maximum of the scanner [64,65]. As our rats exhibited striatal volumes of about 35 to 50 mm<sup>2</sup> [26,66] and the utilized scanner is characterized by a spatial resolution of 1.5 mm, the CPu as the target region exceeded the critical size for the occurrence of PVE. Moreover, the CPu seems to be only minimally effected by extracranial gland and skull activity resulting from its deep localization within the brain [6]. Due to predominantly relative comparisons between hemispheres within treatment groups in our study setup, a potentially emerging PVE would be mathematically shortened. Altogether, in this study we decided to omit PVE correction for quantification of [<sup>18</sup>F]fallypride uptake in the CPu of hemi-PD rats. Also in comparable studies, no correction of the PVE seemed necessary for quantification of radioligands demonstrating very specific and region-limited binding kinetics like [<sup>18</sup>F]fallypride [2] or [<sup>11</sup>C]raclopride [67]. Nevertheless, a methodical consideration of this aspect might be of high interest for further investigations. Another critical point of small animal imaging is the need for anesthesia, commonly realized by respiration of isoflurane. For analyzing the availability of D<sub>2</sub>/D<sub>3</sub>R effects of isoflurane seem not pivotal, as the BP of D<sub>2</sub>R measured with [<sup>11</sup>C]raclopride was only marginally changed in mice [5] and [<sup>18</sup>F]fallypride uptake did not differ in awake rats that received late isoflurane anesthesia compared to rats under continuous anesthesia [61].

#### 4. Materials and Methods

##### 4.1. Animals

Twenty-six male Wistar rats (Charles River WIGA, Sulzfeld, Germany; RRID: RGD\_737929) either assigned to controls (sham-6-OHDA + sham-BoNT-A, *n* = 9), sham-injected hemi-PD rats (6-OHDA + sham-BoNT-A, *n* = 7) or BoNT-A-injected hemi-PD rats (6-OHDA + BoNT-A, *n* = 10) were included in the experiments. Housing was conducted under standard conditions (22 ± 2 °C, 12 h day-and-night cycle) in a fully air-conditioned room with access to water and food ad libitum. The research protocol and all experimental procedures fulfilled legal obligations of the animal welfare act and were approved by the state Animal Research Committee of Mecklenburg–Western Pomerania (LALLF M-V/7221.3-1-005/16, approval: 03/08/2016). The timeline of the experimental setup is presented in Figure 6.

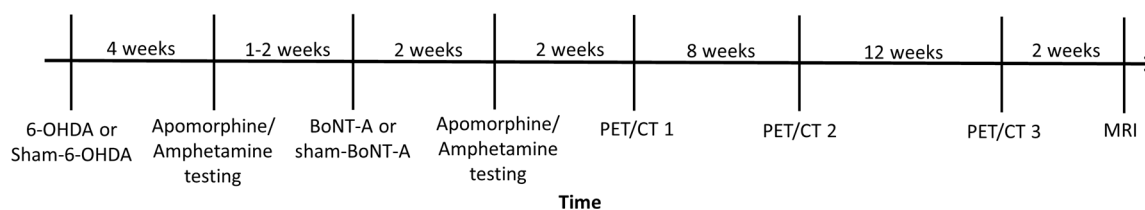


**Figure 6.** Timeline of the study design. Hemi-PD was unilaterally induced by 6-OHDA injection into the right MFB. Controls received sham-6-OHDA injection. The degree of dopaminergic cell loss was verified with apomorphine- and amphetamine-induced behavioral testing. Five to six weeks after the 6-OHDA or sham-6-OHDA injection, rats obtained BoNT-A or sham-BoNT-A injection into the ipsilateral CPu. The positive effect on the motor behavior of BoNT-A was then controlled in rotation tests. Subsequently, each rat was scanned by [<sup>18</sup>F]fallypride-PET/CT analysis one, three and six months post-BoNT-A or -sham-BoNT-A injection. A final MRI scan was performed as anatomical reference for PET/CT imaging.

#### 4.2. 6-OHDA and BoNT-A Injection

Animals received 6-OHDA or sham-6-OHDA injection at a weight of 285–305 g in a stereotaxic operation and BoNT-A or sham-BoNT-A injection five to six weeks later. Anesthesia was induced with a ketamine-xylazine mixture (ketamine: 50 mg/kg, xylazine: 4 mg/kg). Dopaminergic cell death was provoked by unilateral injection of 24 µg of 6-OHDA (Sigma-Aldrich, St. Louis, MO, USA) dissolved in 4 µL 0.1 M citrate buffer into the right MFB. Sham-6-OHDA animals received only citrate buffer. Exact coordinates of 6-OHDA or sham-6-OHDA injection were anterior-posterior = −2.3 mm, lateral = −1.5 mm and ventral = −9.0 mm [68]. BoNT-A (Lot#13029A1; List, Campbell, CA, USA; purchased via Quadragech, Epsom, UK) supplemented with phosphate-buffered saline (PBS) and 0.1% bovine serum albumin (BSA) was injected at two sites into the right CPu (total dose: 1 ng). Sham-BoNT-A animals received only PBS + BSA. Exact coordinates of BoNT-A or sham-BoNT-A injection were anterior-posterior = +1.3 mm/−0.4 mm, lateral = −2.6 mm/−3.6 mm and ventral = −5.5 mm/−5.5 mm [68]. For application of either 6-OHDA, BoNT-A or sham solution a 5 µL Hamilton syringe was used and the respective volume was continuously delivered over a time span of 4 min. Afterwards, the needle was left in place for another 5 min to avoid reflux.

#### 4.3. Immunohistochemistry

Serial brain sections showing CPu and SN were immunohistochemically reacted for TH to verify successful 6-OHDA lesioning and to exclude an additive effect of BoNT-A. Brains were fixed with 3.7% paraformaldehyde overnight and stained with monoclonal mouse anti-TH antibody (clone TH2, Sigma-Aldrich) following biotinylated horse anti-mouse IgG (Vector Laboratories, Burlingame, CA, USA, 1:67). For details of the procedure see [69].

#### 4.4. Behavioral Testing

The degree of dopaminergic cell loss and the positive motor effect of BoNT-A was evaluated using apomorphine- and amphetamine-induced rotational behavior. Testing was performed in a rotometer [41] four weeks after 6-OHDA or sham-6-OHDA injection and again two weeks after BoNT-A or sham-BoNT-A injection (Figure 6). Drugs were solved in 0.9% NaCl and injected i.p. (apomorphine: 0.25 mg/kg, amphetamine: 2.5 mg/kg). Following apomorphine injection and a waiting time of 5 min to ensure cerebral uptake, rotations were monitored for 40 min. Rotational behavior induced by amphetamine application was analyzed after a waiting time of 15 min throughout a period of 60 min.

#### 4.5. Radioligand Preparation and PET/CT Imaging

Synthesis of [<sup>18</sup>F]fallypride ([<sup>18</sup>F](S)-N-((1-allylpyrrolidin-2-yl)methyl-5-(3-fluoropropyl)-2,3-dimethoxybenzamide) and semi-preparative HPLC for purification was conducted according to the protocol of [70], followed by an extensive quality control. D<sub>2</sub>/D<sub>3</sub>R availability was analyzed by dynamic [<sup>18</sup>F]fallypride PET/CT imaging over 90 min, each animal was measured one, three, and six months post-BoNT-A or -sham-BoNT-A injection. Anesthesia was initially administered with 5% isoflurane (AbbVie, North Chicago, IL, USA) vaporized in oxygen gas and maintained during scanning time with 1.5–3%. Body temperature was held constant at 38 °C via a heating pad and respiration rate of the animals was monitored throughout the PET/CT measurement. Each rat was placed in head-prone position centered in the field of view of a commercially available preclinical PET/CT scanner (Inveon<sup>®</sup>, Siemens Healthcare, Knoxville, TN, USA); performance evaluation of the system was described by [71,72]. [<sup>18</sup>F]fallypride was injected as a bolus over 1 min via a microcatheter into the lateral tail vein in a mean dose of 23.44 ± 1.75/24.06 ± 1.76/22.81 ± 2.03 MBq (sham-6-OHDA + sham-BoNT-A), PET/CT 1-3), 24.52 ± 2.48, 23.84 ± 2.28, 23.88 ± 2.46 MBq (6-OHDA + Sham-BoNT-A, PET/CT 1-3) and 22.99 ± 2.50, 22.55 ± 3.93, 21.61 ± 2.27 MBq (6-OHDA + BoNT-A, PET/CT 1-3). The acquisition of dynamic PET as list mode data set was started immediately with the injection. PET studies were

reconstructed as series 3D PET images of multiple frames with various time durations ( $6 \times 10$  s,  $8 \times 30$  s,  $5 \times 300$  s,  $5 \times 1800$  s) with a voxel size of  $0.86 \text{ mm} \times 0.86 \text{ mm} \times 0.79 \text{ mm}$  using a 2D-ordered subsets expectation maximization algorithm (four iterations, six subsets). Attenuation correction was performed on the basis of whole body CT scan and PET studies were also corrected for random coincidences, dead time, scatter and radioactive decay.

#### 4.6. MRI Imaging

MRI was performed on anesthetized rats (1.5–3% isoflurane in oxygen) at least 10 days after the last PET/CT examination and about eight months post-6-OHDA lesion. MRI of the rats was conducted using a 7 Tesla small animal MRI scanner (BioSpec 70/30 AVANCE III, 7.0 T, 440 mT/m gradient strength, Paravision software v6.01., Bruker BioSpin MRI GmbH, Ettlingen, Germany) with a 1 H transmit resonator (inner diameter: 86 mm; vendor type-nr.: T12053V3, Bruker, Ettlingen, Germany) and a receive-only surface coil array ( $2 \times 2$  array rat brain coil; vendor type-nr.: T11483V3, Bruker) positioned on the head of the rats. The imaging protocol included 3D isotropic T1w FLASH imaging sequences with transversal slice orientation, 8/45 ms TE/TR,  $35 \text{ mm} \times 35 \text{ mm} \times 16 \text{ mm}$  FOV,  $200 \mu\text{m} \times 200 \mu\text{m} \times 200 \mu\text{m}$  resolution,  $175 \text{ pixel} \times 175 \text{ pixel} \times 80 \text{ pixel}$  matrix size,  $20^\circ$  flip angle, 12:36 min:sec acquisition time, one average and fat suppression.

#### 4.7. Image Analysis

For qualitative and quantitative analysis PMOD v3.7 (PMOD Technologies LLC, Zurich, Switzerland) was used. Qualitative assessment was conducted with parametric maps of the spatial  $BP_{nd}$  distribution by pixel-wised calculation (extracting signals from individual pixels). For determination of  $BP_{nd}$ , delineation of the target region (left and right striatum) as well as the reference region (cerebellum) was conducted using an implemented MRI-based rat brain atlas [73]. Therefore, PET data were first transformed to the standard matrix of the animal-specific MRI (3D isotropic T1w FLASH). Two rats did not receive a MRI scan, for transformation a representative MRI of the same experimental group was used. Two animals died during the study course and four PET/CT scanning time points were canceled. Six PET/CT scans were excluded from analysis due to incorrect injection of the radioligand and one due to development of a brain tumor (Table 1). Animal-specific MRI datasets were then transformed to Schiffer matrix and the respective transformation matrix was saved. In a final step, PET data were transformed into a Schiffer matrix using the saved transformation matrix to guarantee maximal resolution of PET data (Figure 7a,b). All transformations were performed using ridged matching method implemented in PMOD. VOIs for target and reference region were then defined with the Schiffer atlas [73] (Figure 7c,d) and time–activity curves (TAC) were extracted from dynamic PET data. For kinetic analysis the model-driven SRTM2 [54] was applied and  $BP_{nd}$  was estimated, being defined as the ratio of receptor density ( $B_{max}$ ) multiplied by the radioligand affinity [74]. We assumed that receptor affinity was not changed in 6-OHDA-lesion rats compared to controls as  $BP$  of [ $^{18}\text{F}$ ]fallypride is resistant to DA depletion [75–77].

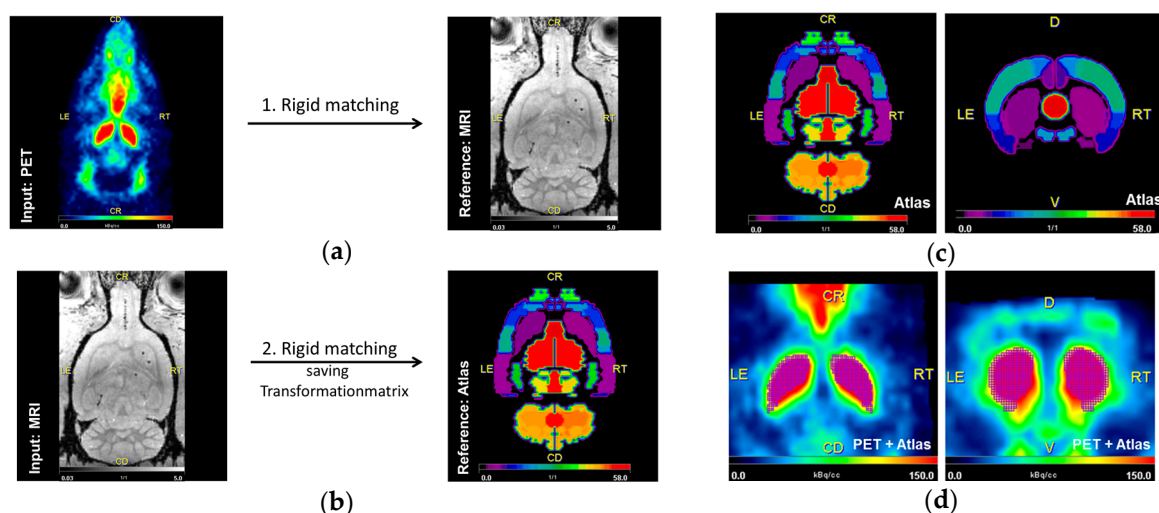


**Figure 7.** (a,b) Workflow of the transformation process using rigid matching. In a first step PET (input) was transformed to the matrix of the animal-specific MRI (reference) (a). Secondly, the animal-specific MRI (input) was transformed to the matrix of the Schiffer atlas and the transformation matrix was saved and finally applied to PET data (b). (c,d) Example of the delineation of the left and right striatum (purple grid) and the cerebellum (orange grid) in PET (d) with published Schiffer atlas (c) in a control animal (sham-6-OHDA + sham-BoNT-A).

#### 4.8. Statistical Assessment

Statistical significance was examined using IBM SPSS Statistics software version 22. To test for the Gaussian distribution of all reported data, a Kolmogorov–Smirnov test was performed followed by a univariate general linear model. Between-subjects post hoc ANOVA analysis of variance was conducted with  $D_2/D_3R$  availability of the CPu (left/right) as the dependent variable and the experimental group as covariate. Following, Bonferroni correction with the factor group for each of the analyzed time points was performed ( $df = 5$ ; ( $F = 4.598$  one month post-BoNT-A or -sham-BoNT-A;  $F = 3.051$  three months post-BoNT-A or -sham-BoNT-A,  $F = 2.584$  six months post-BoNT-A or -sham-BoNT-A)). Statistical significance of apomorphine- and amphetamine-induced behavior was analyzed by the unpaired student's *t*-test. To analyze correlations of  $D_2/D_3R$  availability and rotational behavior in the apomorphine-induced rotation test linear regression followed by a two-sided Pearson correlation test was implemented. A *p*-value below 0.05 was considered to indicate significance.

## 5. Conclusions

We here provide a longitudinal study on changes of  $D_2/D_3R$  availability in the 6-OHDA-induced hemi-PD rat model. We found an increase in  $D_2/D_3R$  availability of 23% up to six months post-lesion, which was significantly reduced after striatal injection of BoNT-A. Interestingly, this decrease of pathological  $D_2/D_3R$  imbalance by intrastriatal BoNT-A injection significantly correlated with behavior in the apomorphine rotation test. Altogether, our results emphasize the therapeutical capability of BoNT-A in hemi-PD rats and provide insights in the underlying mechanisms.

**Acknowledgments:** The authors would like to thank Anne Möller, Joanna Förster, and Susann Lehmann for their technical assistance. We gratefully acknowledge Susann Lehmann, Iloana Klamfuß, Petra Wolff, Robin Piecha, Mathias Lietz, and Ulf Hasse for animal housing and care. We appreciate financial support by Deutsche Forschungsgemeinschaft and Universität Rostock/Universitätsmedizin Rostock within the funding program Open Access Publishing.

**Author Contributions:** Teresa Mann, Andreas Wree, Jens Kurth, and Tobias Lindner wrote the manuscript. Andreas Wree and Bernd Joachim Krause planned the project and Jens Kurth provided the analyzing strategy. Andreas Wree, Alexander Hawlitschka, and Teresa Mann executed stereotaxic operations. Teresa Mann analyzed

data and designed figures. Teresa Mann and Alexander Hawlitschka conducted rotation tests with apomorphine and amphetamine. Alexander Hawlitschka performed TH immunostaining. Jan Stenzel planned and performed PET/CT scans. Tobias Lindner and Stefan Polei determined the MRI protocol and conducted measurements. Alexander Hohn established the synthesis protocol and synthesized the radioligand [<sup>18</sup>F]fallypride. All authors contributed substantially to the project and the manuscript.

**Conflicts of Interest:** The authors declare no conflict of interest. The founding sponsors had no role in the design of the study; in the collection, analyses, or interpretation of data; in the writing of the manuscript, and in the decision to publish the results.

## Abbreviations

BSA	Bovine serum albumin
BP <sub>nd</sub>	non-displaceable binding potential
BoNT-A	Botulinum neurotoxin A
CPu	caudate–putamen
D <sub>2</sub> /D <sub>3</sub> R	D <sub>2</sub> /D <sub>3</sub> receptor
DA	dopamine
hemi-PD	hemiparkinsonian
MFB	medial forebrain bundle
MRI	magnetic resonance imaging
MSN	medium spiny neuron
PD	Parkinson’s disease
PET	positron emission tomography
PBS	phosphate-buffered saline
PVE	partial volume effect
SNAP25	synaptosomal-associated protein of 25-kDa
SN(pc)	substantia nigra (pars compacta)
SRTM2	simplified reference tissue model 2
TAC	time-activity curve
TH	tyrosine hydroxylase
VOI	voxels of interest
6-OHDA	6-hydroxydopamine

## References

1. Vučković, M.G.; Li, Q.; Fisher, B.; Nacca, A.; Leahy, R.M.; Walsh, J.P.; Mukherjee, J.; Williams, C.; Jakowec, M.W.; Petzinger, G.M. Exercise elevates dopamine D2 receptor in a mouse model of Parkinson’s disease: In vivo imaging with [<sup>18</sup>F]fallypride. *Mov. Disord.* **2010**, *25*, 2777–2784. [[CrossRef](#)] [[PubMed](#)]
2. Choi, J.Y.; Kim, C.H.; Jeon, T.J.; Cho, W.G.; Lee, J.S.; Lee, S.J.; Choi, T.H.; Kim, B.S.; Yi, C.H.; Seo, Y.; et al. Evaluation of dopamine transporters and D2 receptors in hemiparkinsonian rat brains in vivo using consecutive PET scans of [<sup>18</sup>F]FPCIT and [<sup>18</sup>F]fallypride. *Appl. Radiat. Isot.* **2012**, *70*, 2689–2694. [[CrossRef](#)] [[PubMed](#)]
3. Wedekind, F.; Oskamp, A.; Lang, M.; Hawlitschka, A.; Zilles, K.; Wree, A.; Bauer, A. Intra-striatal administration of botulinum neurotoxin A normalizes striatal D2 R binding and reduces striatal D1 R binding in male hemiparkinsonian rats. *J. Neurosci. Res.* **2018**, *96*, 75–86. [[CrossRef](#)] [[PubMed](#)]
4. Mukherjee, J.; Christian, B.T.; Narayanan, T.K.; Shi, B.; Mantil, J. Evaluation of dopamine D-2 receptor occupancy by clozapine, risperidone, and haloperidol in vivo in the rodent and nonhuman primate brain using 18F-fallypride. *Neuropsychopharmacology* **2001**, *25*, 476–488. [[CrossRef](#)]
5. Honer, M.; Brühlmeier, M.; Missimer, J.; Schubiger, A.P.; Ametamey, S.M. Dynamic imaging of striatal D2 receptors in mice using quad-HIDAC PET. *J. Nucl. Med.* **2004**, *45*, 464–470. [[PubMed](#)]
6. Mukherjee, J.; Constantinescu, C.C.; Hoang, A.T.; Jerjian, T.; Majji, D.; Pan, M.-L. Dopamine D3 receptor binding of <sup>18</sup>F-fallypride: Evaluation using in vitro and in vivo PET imaging studies. *Synapse* **2015**, *69*, 577–591. [[CrossRef](#)] [[PubMed](#)]



7. Ding, J.; Guzman, J.N.; Tkatch, T.; Chen, S.; Goldberg, J.A.; Ebert, P.J.; Levitt, P.; Wilson, C.J.; Hamm, H.E.; Surmeier, D.J. RGS4-dependent attenuation of M4 autoreceptor function in striatal cholinergic interneurons following dopamine depletion. *Nat. Neurosci.* **2006**, *9*, 832–842. [[CrossRef](#)] [[PubMed](#)]
8. Pisani, A.; Bonsi, P.; Centonze, D.; Gubellini, P.; Bernardi, G.; Calabresi, P. Targeting striatal cholinergic interneurons in Parkinson's disease: Focus on metabotropic glutamate receptors. *Neuropharmacology* **2003**, *45*, 45–56. [[CrossRef](#)]
9. Goldberg, J.A.; Ding, J.B.; Surmeier, D.J. Muscarinic modulation of striatal function and circuitry. *Handb. Exp. Pharmacol.* **2012**, 223–241. [[CrossRef](#)]
10. Zhou, F.M.; Liang, Y.; Dani, J. A Endogenous nicotinic cholinergic activity regulates dopamine release in the striatum. *Nat. Neurosci.* **2001**, *4*, 1224–1229. [[CrossRef](#)] [[PubMed](#)]
11. Threlfell, S.; Clements, M.A.; Khodai, T.; Pienaar, I.S.; Exley, R.; Wess, J.; Cragg, S.J. Striatal muscarinic receptors promote activity dependence of dopamine transmission via distinct receptor subtypes on cholinergic interneurons in ventral versus dorsal striatum. *J. Neurosci.* **2010**, *30*, 3398–3408. [[CrossRef](#)] [[PubMed](#)]
12. Duty, S.; Jenner, P. Animal models of Parkinson's disease: A source of novel treatments and clues to the cause of the disease. *Br. J. Pharmacol.* **2011**, *164*, 1357–1391. [[CrossRef](#)] [[PubMed](#)]
13. Soto-Otero, R.; Méndez-Alvarez, E.; Hermida-Ameijeiras, A.; Muñoz-Patiño, A.M.; Labandeira-Garcia, J.L. Autoxidation and neurotoxicity of 6-hydroxydopamine in the presence of some antioxidants: Potential implication in relation to the pathogenesis of Parkinson's disease. *J. Neurochem.* **2000**, *74*, 1605–1612. [[CrossRef](#)] [[PubMed](#)]
14. Bové, J.; Perier, C. Neurotoxin-based models of Parkinson's disease. *Neuroscience* **2012**, *211*, 51–76. [[CrossRef](#)] [[PubMed](#)]
15. Carlsson, A.; Lindqvist, M.; Magnusson, T. 3,4-Dihydroxyphenylalanine and 5-hydroxytryptophan as reserpine antagonists. *Nature* **1957**, *180*, 1200. [[CrossRef](#)] [[PubMed](#)]
16. Cacabelos, R. Parkinson's Disease: From Pathogenesis to Pharmacogenomics. *Int. J. Mol. Sci.* **2017**, *18*, 551. [[CrossRef](#)] [[PubMed](#)]
17. Moritz, A.E.; Benjamin Free, R.; Sibley, D.R. Advances and challenges in the search for D2 and D3 dopamine receptor-selective compounds. *Cell. Signal.* **2018**, *41*, 75–81. [[CrossRef](#)] [[PubMed](#)]
18. Olanow, C.W.; Stocchi, F. Levodopa: A new look at an old friend. *Mov. Disord.* **2017**. [[CrossRef](#)] [[PubMed](#)]
19. Kühn, J.; Haumesser, J.K.; Beck, M.H.; Altschüler, J.; Kühn, A.A.; Nikulin, V.V.; van Riesen, C. Differential effects of levodopa and apomorphine on neuronal population oscillations in the cortico-basal ganglia loop circuit in vivo in experimental parkinsonism. *Exp. Neurol.* **2017**, *298*, 122–133. [[CrossRef](#)]
20. Horstink, M.; Tolosa, E.; Bonuccelli, U.; Deuschl, G.; Friedman, A.; Kanovsky, P.; Larsen, J.P.; Lees, A.; Oertel, W.; Poewe, W.; et al. Review of the therapeutic management of Parkinson's disease. Report of a joint task force of the European Federation of Neurological Societies and the Movement Disorder Society-European Section. Part I: Early (uncomplicated) Parkinson's disease. *Eur. J. Neurol.* **2006**, *13*, 1170–1185. [[CrossRef](#)] [[PubMed](#)]
21. Horstink, M.; Tolosa, E.; Bonuccelli, U.; Deuschl, G.; Friedman, A.; Kanovsky, P.; Larsen, J.P.; Lees, A.; Oertel, W.; Poewe, W.; et al. Review of the therapeutic management of Parkinson's disease. Report of a joint task force of the European Federation of Neurological Societies (EFNS) and the Movement Disorder Society-European Section (MDS-ES). Part II: Late (complicated) Parkinson's disease. *Eur. J. Neurol.* **2006**, *13*, 1186–1202. [[CrossRef](#)] [[PubMed](#)]
22. Fernandez, H.H. Updates in the medical management of Parkinson disease. *Clevel. Clin. J. Med.* **2012**, *79*, 28–35. [[CrossRef](#)] [[PubMed](#)]
23. Wree, A.; Mix, E.; Hawlitschka, A.; Antipova, V.; Witt, M.; Schmitt, O.; Benecke, R. Intrastriatal botulinum toxin abolishes pathologic rotational behaviour and induces axonal varicosities in the 6-OHDA rat model of Parkinson's disease. *Neurobiol. Dis.* **2011**, *41*, 291–298. [[CrossRef](#)] [[PubMed](#)]
24. Holzmann, C.; Dräger, D.; Mix, E.; Hawlitschka, A.; Antipova, V.; Benecke, R.; Wree, A. Effects of intrastriatal botulinum neurotoxin A on the behavior of Wistar rats. *Behav. Brain Res.* **2012**, *234*, 107–116. [[CrossRef](#)] [[PubMed](#)]
25. Hawlitschka, A.; Antipova, V.; Schmitt, O.; Witt, M.; Benecke, R.; Mix, E.; Wree, A. Intracerebrally applied botulinum neurotoxin in experimental neuroscience. *Curr. Pharm. Biotechnol.* **2013**, *14*, 124–130. [[PubMed](#)]

26. Antipova, V.; Hawlitschka, A.; Mix, E.; Schmitt, O.; Dräger, D.; Benecke, R.; Wree, A. Behavioral and structural effects of unilateral intrastriatal injections of botulinum neurotoxin a in the rat model of Parkinson's disease. *J. Neurosci. Res.* **2013**, *91*, 838–847. [[CrossRef](#)] [[PubMed](#)]
27. Caleo, M.; Antonucci, F.; Restani, L.; Mazzocchio, R. A reappraisal of the central effects of botulinum neurotoxin type A: By what mechanism? *J. Neurochem.* **2009**, *109*, 15–24. [[CrossRef](#)] [[PubMed](#)]
28. Binz, T.; Sikorra, S.; Mahrhold, S. Clostridial neurotoxins: Mechanism of SNARE cleavage and outlook on potential substrate specificity reengineering. *Toxins* **2010**, *2*, 665–682. [[CrossRef](#)] [[PubMed](#)]
29. Kroken, A.R.; Karalewitz, A.P.-A.; Fu, Z.; Kim, J.-J.P.; Barbieri, J.T. Novel ganglioside-mediated entry of botulinum neurotoxin serotype D into neurons. *J. Biol. Chem.* **2011**, *286*, 26828–26837. [[CrossRef](#)] [[PubMed](#)]
30. Mehlan, J.; Brosig, H.; Schmitt, O.; Mix, E.; Wree, A.; Hawlitschka, A. Intrastriatal injection of botulinum neurotoxin-A is not cytotoxic in rat brain—A histological and stereological analysis. *Brain Res.* **2016**, *1630*, 18–24. [[CrossRef](#)] [[PubMed](#)]
31. Mann, T.; Zilles, K.; Dikow, H.; Hellfrisch, A.; Cremer, M.; Piel, M.; Rösch, F.; Hawlitschka, A.; Schmitt, O.; Wree, A. Dopamine, Noradrenaline and Serotonin Receptor Densities in the Striatum of Hemiparkinsonian Rats following Botulinum Neurotoxin-A Injection. *Neuroscience* **2018**, *374*, 187–204. [[CrossRef](#)] [[PubMed](#)]
32. Grossman, R.; Paden, C.M.; Fry, P.A.; Rhodes, R.S.; Biegon, A. Persistent region-dependent neuroinflammation, NMDA receptor loss and atrophy in an animal model of penetrating brain injury. *Future Neurol.* **2012**, *7*, 329–339. [[CrossRef](#)] [[PubMed](#)]
33. Qü, M.; Buchkremer-Ratzmann, I.; Schiene, K.; Schroeter, M.; Witte, O.W.; Zilles, K. Bihemispheric reduction of GABAA receptor binding following focal cortical photothrombotic lesions in the rat brain. *Brain Res.* **1998**, *813*, 374–380. [[CrossRef](#)]
34. Jeon, B.S.; Jackson-Lewis, V.; Burke, R.E. 6-Hydroxydopamine lesion of the rat substantia nigra: Time course and morphology of cell death. *Neurodegeneration* **1995**, *4*, 131–137. [[CrossRef](#)] [[PubMed](#)]
35. Creese, I.; Burt, D.R.; Snyder, S.H. Dopamine receptor binding enhancement accompanies lesion-induced behavioral supersensitivity. *Science* **1977**, *197*, 596–598. [[CrossRef](#)] [[PubMed](#)]
36. Przedbroski, S.; Leviver, M.; Jiang, H.; Ferreira, M.; Jackson-Lewis, V.; Donaldson, D.; Togasaki, D.M. Dose-dependent lesions of the dopaminergic nigrostriatal pathway induced by intrastriatal injection of 6-hydroxydopamine. *Neuroscience* **1995**, *67*, 631–647. [[CrossRef](#)]
37. Sun, W.; Sugiyama, K.; Asakawa, T.; Yamaguchi, H.; Akamine, S.; Ouchi, Y.; Magata, Y.; Namba, H. Dynamic changes of striatal dopamine D2 receptor binding at later stages after unilateral lesions of the medial forebrain bundle in Parkinsonian rat models. *Neurosci. Lett.* **2011**, *496*, 157–162. [[CrossRef](#)] [[PubMed](#)]
38. Ungerstedt, U.; Butcher, L.L.; Butcher, S.G.; Andén, N.E.; Fuxe, K. Direct chemical stimulation of dopaminergic mechanisms in the neostriatum of the rat. *Brain Res.* **1969**, *14*, 461–471. [[CrossRef](#)]
39. Ma, Y.; Zhan, M.; OuYang, L.; Li, Y.; Chen, S.; Wu, J.; Chen, J.; Luo, C.; Lei, W. The effects of unilateral 6-OHDA lesion in medial forebrain bundle on the motor, cognitive dysfunctions and vulnerability of different striatal interneuron types in rats. *Behav. Brain Res.* **2014**, *266*, 37–45. [[CrossRef](#)] [[PubMed](#)]
40. Wang, Q.; Wei, X.; Gao, H.; Li, J.; Liao, J.; Liu, X.; Qin, B.; Yu, Y.; Deng, C.; Tang, B.; et al. Simvastatin reverses the downregulation of M1/4 receptor binding in 6-hydroxydopamine-induced parkinsonian rats: The association with improvements in long-term memory. *Neuroscience* **2014**, *267*, 57–66. [[CrossRef](#)] [[PubMed](#)]
41. Ungerstedt, U.; Arbuthnott, G.W. Quantitative recording of rotational behavior in rats after 6-hydroxy-dopamine lesions of the nigrostriatal dopamine system. *Brain Res.* **1970**, *24*, 485–493. [[CrossRef](#)]
42. Hudson, J.L.; van Horne, C.G.; Strömberg, I.; Brock, S.; Clayton, J.; Masserano, J.; Hoffer, B.J.; Gerhardt, G.A. Correlation of apomorphine- and amphetamine-induced turning with nigrostriatal dopamine content in unilateral 6-hydroxydopamine lesioned rats. *Brain Res.* **1993**, *626*, 167–174. [[CrossRef](#)]
43. Ginovart, N.; Farde, L.; Halldin, C.; Swahn, C.G. Effect of reserpine-induced depletion of synaptic dopamine on [<sup>11</sup>C]raclopride binding to D2-dopamine receptors in the monkey brain. *Synapse* **1997**, *25*, 321–325. [[CrossRef](#)]
44. Seeman, P.; Guan, H.C.; Niznik, H.B. Endogenous dopamine lowers the dopamine D2 receptor density as measured by [3H]raclopride: Implications for positron emission tomography of the human brain. *Synapse* **1989**, *3*, 96–97. [[CrossRef](#)] [[PubMed](#)]
45. Young, L.T.; Wong, D.F.; Goldman, S.; Minkin, E.; Chen, C.; Matsumura, K.; Scheffel, U.; Wagner, H.N. Effects of endogenous dopamine on kinetics of [3H]N-methylspiperone and [3H]raclopride binding in the rat brain. *Synapse* **1991**, *9*, 188–194. [[CrossRef](#)] [[PubMed](#)]

46. Staunton, D.A.; Wolfe, B.B.; Groves, P.M.; Molinoff, P.B. Dopamine receptor changes following destruction of the nigrostriatal pathway: Lack of a relationship to rotational behavior. *Brain Res.* **1981**, *211*, 315–327. [[CrossRef](#)]
47. Fornaretto, M.G.; Caccia, C.; Caron, M.G.; Fariello, R.G. Dopamine Receptors Status After Unilateral Nigral 6-OHDA Lesion Hybridization Study in the Rat Brain. *Mol. Chem. Neuropathol.* **1993**, *19*, 147–162. [[CrossRef](#)] [[PubMed](#)]
48. Ryu, J.H.; Yanai, K.; Zhao, X.L.; Watanabe, T. The effect of dopamine D1 receptor stimulation on the up-regulation of histamine H3-receptors following destruction of the ascending dopaminergic neurones. *Br. J. Pharmacol.* **1996**, *118*, 585–592. [[CrossRef](#)] [[PubMed](#)]
49. Araki, T.; Tanji, H.; Kato, H.; Imai, Y.; Mizugaki, M.; Itoyama, Y. Temporal changes of dopaminergic and glutamatergic receptors in 6-hydroxydopamine-treated rat brain. *Eur. Neuropsychopharmacol.* **2000**, *10*, 365–375. [[CrossRef](#)]
50. Xu, Z.C.; Ling, G.; Sahr, R.N.; Neal-Beliveau, B.S. Asymmetrical changes of dopamine receptors in the striatum after unilateral dopamine depletion. *Brain Res.* **2005**, *1038*, 163–170. [[CrossRef](#)] [[PubMed](#)]
51. Inaji, M.; Okauchi, T.; Ando, K.; Maeda, J.; Nagai, Y.; Yoshizaki, T.; Okano, H.; Nariai, T.; Ohno, K.; Obayashi, S.; et al. Correlation between quantitative imaging and behavior in unilaterally 6-OHDA-lesioned rats. *Brain Res.* **2005**, *1064*, 136–145. [[CrossRef](#)] [[PubMed](#)]
52. Hume, S.P.; Opacka-Juffry, J.; Myers, R.; Ahier, R.G.; Ashworth, S.; Brooks, D.J.; Lammertsma, A.A. Effect of L-dopa and 6-hydroxydopamine lesioning on [<sup>11</sup>C]raclopride binding in rat striatum, quantified using PET. *Synapse* **1995**, *21*, 45–53. [[CrossRef](#)] [[PubMed](#)]
53. Zhou, X.; Doorduyn, J.; Elsinga, P.H.; Dierckx, R.A.J.O.; de Vries, E.F.J.; Casteels, C. Altered adenosine 2A and dopamine D2 receptor availability in the 6-hydroxydopamine-treated rats with and without levodopa-induced dyskinesia. *Neuroimage* **2017**, *157*, 209–218. [[CrossRef](#)] [[PubMed](#)]
54. Ariano, M.A.; Stromski, C.J.; Smyk-Randall, E.M.; Sibley, D.R. D2 dopamine receptor localization on striatonigral neurons. *Neurosci. Lett.* **1992**, *144*, 215–220. [[CrossRef](#)]
55. Brock, J.W.; Farooqui, S.; Ross, K.; Prasad, C. Localization of dopamine D2 receptor protein in rat brain using polyclonal antibody. *Brain Res* **1992**, *578*, 244–250. [[CrossRef](#)]
56. Yung, K.K.L.; Bolam, J.P.; Smith, A.D.; Hersch, S.M.; Ciliax, B.J.; Levey, A.I. Immunocytochemical localization of D1 and D2 dopamine receptors in the basal ganglia of the rat: Light and electron microscopy. *Neuroscience* **1995**, *65*, 709–730. [[CrossRef](#)]
57. Wu, Y.; Carson, R.E. Noise reduction in the simplified reference tissue model for neuroreceptor functional imaging. *J. Cerebr. Blood Flow Metab.* **2002**, *22*, 1440–1452. [[CrossRef](#)] [[PubMed](#)]
58. Lammertsma, A.A.; Bench, C.J.; Hume, S.P.; Osman, S.; Gunn, K.; Brooks, D.J.; Frackowiak, R.S. Comparison of methods for analysis of clinical [<sup>11</sup>C]raclopride studies. *J. Cerebr. Blood Flow Metab.* **1996**, *16*, 42–52. [[CrossRef](#)] [[PubMed](#)]
59. Martres, M.P.; Sales, N.; Bouthenet, M.L.; Schwartz, J.C. Localisation and pharmacological characterisation of D-2 dopamine receptors in rat cerebral neocortex and cerebellum using [<sup>125</sup>I]iodosulpride. *Eur. J. Pharmacol.* **1985**, *118*, 211–219. [[CrossRef](#)]
60. Seneca, N.; Finnema, S.J.; Farde, L.; Gulyás, B.; Wikström, H.V.; Halldin, C.; Innis, R.B. Effect of amphetamine on dopamine D2 receptor binding in nonhuman primate brain: A comparison of the agonist radioligand [<sup>11</sup>C]MNPA and antagonist [<sup>11</sup>C]raclopride. *Synapse* **2006**, *59*, 260–269. [[CrossRef](#)] [[PubMed](#)]
61. Constantinescu, C.C.; Coleman, R.A.; Pan, M.-L.; Mukherjee, J. Striatal and extrastriatal microPET imaging of D2/D3 dopamine receptors in rat brain with [<sup>18</sup>F]fallypride and [<sup>18</sup>F]desmethoxyfallypride. *Synapse* **2011**, *65*, 778–787. [[CrossRef](#)] [[PubMed](#)]
62. Yoder, K.K.; Albrecht, D.S.; Kareken, D.A.; Federici, L.M.; Perry, K.M.; Patton, E.A.; Zheng, Q.-H.; Mock, B.H.; O'Connor, S.; Herring, C.M. Test-retest variability of [<sup>11</sup>C]raclopride-binding potential in nontreatment-seeking alcoholics. *Synapse* **2011**, *65*, 553–561. [[CrossRef](#)] [[PubMed](#)]
63. Prieto, E.; Collantes, M.; Delgado, M.; Juri, C.; García-García, L.; Molinet, F.; Fernández-Valle, M.E.; Pozo, M.A.; Gago, B.; Martí-Climent, J.M.; et al. Statistical parametric maps of <sup>18</sup>F-FDG PET and 3-D autoradiography in the rat brain: A cross-validation study. *Eur. J. Nucl. Med. Mol. Imaging* **2011**, *38*, 2228–2237. [[CrossRef](#)] [[PubMed](#)]
64. Hoffman, E.J.; Huang, S.C.; Phelps, M.E. Quantitation in positron emission computed tomography: 1. Effect of object size. *J. Comput. Assist. Tomogr.* **1979**, *3*, 299–308. [[CrossRef](#)] [[PubMed](#)]

65. Hoffman, E.J.; Huang, S.C.; Plummer, D.; Phelps, M.E. Quantitation in positron emission computed tomography: 6. effect of nonuniform resolution. *J. Comput. Assist. Tomogr.* **1982**, *6*, 987–999. [[CrossRef](#)] [[PubMed](#)]
66. Andersson, C.; Hamer, R.M.; Lawler, C.P.; Mailman, R.B.; Lieberman, J.A. Striatal volume changes in the rat following long-term administration of typical and atypical antipsychotic drugs. *Neuropsychopharmacology* **2002**, *27*, 143–151. [[CrossRef](#)]
67. Garcia, D.V.; Casteels, C.; Schwarz, A.J.; Dierckx, R.A.J.O.; Koole, M.; Doorduyn, J. Correction: A Standardized Method for the Construction of Tracer Specific PET and SPECT Rat Brain Templates: Validation and Implementation of a Toolbox. *PLoS ONE* **2015**, *10*, e0143900. [[CrossRef](#)] [[PubMed](#)]
68. Paxinos, G.; Watson, C. *The Rat Brain in Stereotaxic Coordinates*, 6th ed.; Academic press: San Diego, CA, USA, 2007; ISBN 9780125476126.
69. Hawlitschka, A.; Holzmann, C.; Witt, S.; Spiewok, J.; Neumann, A.-M.; Schmitt, O.; Wree, A.; Antipova, V. Intrastratially injected botulinum neurotoxin-A differently effects cholinergic and dopaminergic fibers in C57BL/6 mice. *Brain Res.* **2017**, *1676*, 46–56. [[CrossRef](#)] [[PubMed](#)]
70. Gao, M.; Wang, M.; Mock, B.H.; Glick-Wilson, B.E.; Yoder, K.K.; Hutchins, G.D.; Zheng, Q.-H. An improved synthesis of dopamine D2/D3 receptor radioligands [<sup>11</sup>C]fallypride and [<sup>18</sup>F]fallypride. *Appl. Radiat. Isot.* **2010**, *68*, 1079–1086. [[CrossRef](#)] [[PubMed](#)]
71. Bao, Q.; Newport, D.; Chen, M.; Stout, D.B.; Chatziioannou, A.F. Performance evaluation of the inveon dedicated PET preclinical tomograph based on the NEMA NU-4 standards. *J. Nucl. Med.* **2009**, *50*, 401–408. [[CrossRef](#)] [[PubMed](#)]
72. Kemp, B.J.; Hruska, C.B.; McFarland, A.R.; Lenox, M.W.; Lowe, V.J. NEMA NU 2-2007 performance measurements of the Siemens Inveon preclinical small animal PET system. *Phys. Med. Biol.* **2009**, *54*, 2359–2376. [[CrossRef](#)] [[PubMed](#)]
73. Schiffer, W.K.; Mirrione, M.M.; Biegon, A.; Alexoff, D.L.; Patel, V.; Dewey, S.L. Serial microPET measures of the metabolic reaction to a microdialysis probe implant. *J. Neurosci. Methods* **2006**, *155*, 272–284. [[CrossRef](#)] [[PubMed](#)]
74. Mintun, M.A.; Raichle, M.E.; Kilbourn, M.R.; Wooten, G.F.; Welch, M.J. A quantitative model for the in vivo assessment of drug binding sites with positron emission tomography. *Ann. Neurol.* **1984**, *15*, 217–227. [[CrossRef](#)] [[PubMed](#)]
75. Mukherjee, J.; Yang, Z.-Y.; Lew, R.; Brown, T.; Kronmal, S.; Cooper, M.D.; Seiden, L.S. Evaluation of d-Amphetamine Effects on the Binding of Dopamine D-2 Receptor Radioligand, 18F-Fallypride in Nonhuman Primates Using Positron Emission Tomography. *Synapse* **1997**, *27*, 1–13. [[CrossRef](#)]
76. Cropley, V.L.; Innis, R.B.; Nathan, P.J.; Brown, A.K.; Sangare, J.L.; Lerner, A.; Ryu, Y.H.; Sprague, K.E.; Pike, V.W.; Fujita, M. Small effect of dopamine release and no effect of dopamine depletion on [<sup>18</sup>F]fallypride binding in healthy humans. *Synapse* **2008**, *62*, 399–408. [[CrossRef](#)] [[PubMed](#)]
77. Rominger, A.; Wagner, E.; Mille, E.; Böning, G.; Esmailzadeh, M.; Wängler, B.; Gildehaus, F.-J.; Nowak, S.; Bruche, A.; Tatsch, K.; et al. Endogenous competition against binding of [<sup>18</sup>F]DMFP and [<sup>18</sup>F]fallypride to dopamine D(2/3) receptors in brain of living mouse. *Synapse* **2010**, *64*, 313–322. [[CrossRef](#)] [[PubMed](#)]

**Sample Availability:** Samples of the compounds are not available from the authors.



© 2018 by the authors. Licensee MDPI, Basel, Switzerland. This article is an open access article distributed under the terms and conditions of the Creative Commons Attribution (CC BY) license (<http://creativecommons.org/licenses/by/4.0/>).